



Cite this: *Nanoscale*, 2016, **8**, 18021

Received 5th July 2016,

Accepted 2nd September 2016

DOI: 10.1039/c6nr05330k

[www.rsc.org/nanoscale](http://www.rsc.org/nanoscale)

## Solution-processed highly bright and durable cesium lead halide perovskite light-emitting diodes†

Zhanhua Wei,<sup>\*‡a,c</sup> Ajay Perumal,<sup>‡b</sup> Rui Su,<sup>a</sup> Shendre Sushant,<sup>b</sup> Jun Xing,<sup>a</sup> Qing Zhang,<sup>a</sup> Swee Tiam Tan,<sup>b</sup> Hilmi Volkan Demir<sup>\*b</sup> and Qihua Xiong<sup>\*a</sup>

Recently, CsPbBr<sub>3</sub> perovskites have been emerging as very promising green emission materials for light-emitting diodes (LEDs) due to their high color purity, low cost and high photoluminescence quantum yield (PLQY). However, the corresponding LED performance is still low and far behind CH<sub>3</sub>NH<sub>3</sub>PbBr<sub>3</sub>; it is due to the lack of proper perovskite film preparation methods and interfacial engineering. Herein, we report highly bright and durable CsPbBr<sub>3</sub>-based LEDs fabricated using a one-step solution method. The precursor solution is prepared by simply dissolving CsPbBr<sub>3</sub> powder and a CsBr additive in dimethyl sulfoxide (DMSO). We find that the CsBr additive not only significantly enhances the PLQY but also induces directional crystal growth into micro-plates, forming a smooth perovskite film for LEDs. LEDs employing such high quality films show a high luminance of 7276 cd m<sup>-2</sup> and high color purity with a full width at half maximum of 18 nm. Furthermore, the as-fabricated LEDs reveal an outstanding ambient stability with a decent luminance output (>100 cd m<sup>-2</sup>, steady increase without any degradation trend) for at least 15 h under a constant driving current density (66.7 mA cm<sup>-2</sup>). And we propose two reasons for this unique luminance increasing behavior: (1) the CsPbBr<sub>3</sub> perovskite is thermally stable and can survive from joule heat; and (2) on the other hand, the joule heating will induce interface or crystal-line film annealing, reduce device resistance and then enhance the luminance output.

Inorganic/organic hybrid perovskites have emerged as a prominent light harvester for novel high efficiency solid-state solar

cells, with a recently reported power conversion efficiency of over 22%.<sup>1–3</sup> Recently, perovskite materials are found to be ideal emission materials and intensely investigated as emission layers in light-emitting diodes (LEDs) due to their low cost, color tunability, high photoluminescence quantum yield (PLQY) and narrow emission peak.<sup>4–9</sup> Recently, Lee *et al.* have successfully boosted the current efficiency (CE) of inorganic/organic perovskite (CH<sub>3</sub>NH<sub>3</sub>PbBr<sub>3</sub>) LEDs to 42.9 cd A<sup>-1</sup> in late 2015, indicating that perovskite-based LEDs can be as efficient and promising as the commercial phosphorescent organic light-emitting diodes (OLEDs).<sup>10,11</sup> Constrained by the material traits, ambient stability is an equally important challenge for the further development of potential perovskite-based LED applications. However, there are very few studies which reported the stability performance of perovskite-based LEDs,<sup>4</sup> and it is even more challenging to address the long-term stability.

It is well known that in perovskite solar cells, the organic components in the classical inorganic/organic perovskite materials (MAPbX<sub>3</sub>, MA = CH<sub>3</sub>NH<sub>3</sub>, X = Cl, Br and I) are very sensitive to moisture and heat, *i.e.*, poor humidity and thermal stability,<sup>12–15</sup> which may also induce poor stability in perovskite-based LEDs. Very recently, cation engineering for perovskites, such as adding formamidinium (FA)<sup>2</sup> or Cs<sup>16–18</sup> to replace MA, is found to be an effective strategy to improve thermal and humidity stability of perovskite solar cells. In other words, this kind of cation engineering (partial replacement) or even cation replacement (all inorganic perovskites) could be possibly beneficial for fabricating high performance perovskite LEDs with good stability.

Herein, we report all-inorganic perovskite (CsPbBr<sub>3</sub>) based LEDs with outstanding ambient stability, high brightness (7276 cd m<sup>-2</sup>) and color purity (full width at half maximum, FWHM, 18 nm), which excel benchmarks from previous reports.<sup>4,5,19,20</sup> When the as-fabricated LED devices were driven with a constant current (corresponding to an initial luminance of around 100 cd m<sup>-2</sup>), we observed an unexpected luminance increase instead of degradation. In more detail, during the initial 15 h of the test, the luminance grows from

<sup>a</sup>Division of Physics and Applied Physics, School of Physical and Mathematical Sciences, Nanyang Technological University, Singapore 637371, Singapore.

E-mail: qihua@ntu.edu.sg

<sup>b</sup>Luminous! Centre of Excellence for Semiconductor Lighting and Displays, School of Electrical and Electronic Engineering, Nanyang Technological University, Singapore 639798, Singapore. E-mail: hvdemir@ntu.edu.sg

<sup>c</sup>College of Materials Science & Engineering, Huaqiao University, Xiamen, Fujian, 361021 China. E-mail: weizhanhua@hqu.edu.cn

†Electronic supplementary information (ESI) available. See DOI: 10.1039/c6nr05330k

‡These authors contributed equally to this work.

100 cd m<sup>-2</sup> to ~400 cd m<sup>-2</sup>, indicating considerably stable performance, which is no doubt an important advance in developing practical perovskite-based LEDs for daily life.

One of the most attractive features of the inorganic/organic perovskite-based devices (MAPbX<sub>3</sub> and FAPbX<sub>3</sub>) is their solution-processed capability. Thus, one can prepare a perovskite-based precursor solution with various recipes to achieve a high quality solid perovskite thin film by spin-coating or other methods.<sup>21</sup> In the past few years, the photovoltaic efficiency of perovskite devices increased rapidly by engineering the precursor solution, like solvent engineering<sup>12,22</sup> and compositional engineering.<sup>1,2,10</sup> In other words, the recipe development of a perovskite-based precursor solution plays a key role in pursuing highly efficient perovskite-based devices. However, due to the limited solubility of CsX (X = Cl, Br and I), one cannot prepare a transparent precursor solution by simply dissolving PbX<sub>2</sub> and CsX in certain solutions (*N,N*-dimethylformamide (DMF), dimethyl sulfoxide (DMSO) or their mixtures). To date, the advanced solution process engineering methods (single step methods) have not been applied to all inorganic perovskites. Alternatively, there are two methods developed recently to prepare all-inorganic perovskite thin films, *i.e.*, the two-step method<sup>17,23</sup> and the nanoparticle ink method.<sup>24–26</sup> The two-step method is similar to the previously reported sequential deposition method for CH<sub>3</sub>NH<sub>3</sub>PbI<sub>3</sub> thin films,<sup>27</sup> *i.e.*, a PbBr<sub>2</sub> thin film is firstly prepared by spin-coating using PbBr<sub>2</sub>–DMF solution, then the as-prepared PbBr<sub>2</sub> thin film is dripped in a hot CsX methanol solution and converted into CsPbX<sub>3</sub>.<sup>17,18</sup> The nanoparticle ink method is used to prepare CsPbX<sub>3</sub> nanocrystals (NCs) or quantum dots (QDs) firstly, and then the perovskite thin films can be prepared by spin-coating using the as-prepared nanoparticle colloid solution.<sup>24,25</sup> In this work, we show that the CsPbBr<sub>3</sub> thin film can be simply prepared *via* spin-coating using a one-step solution method, which is more controllable and convenient than the above two methods.

Fig. 1a schematically shows the process of preparing a CsPbBr<sub>3</sub> thin film by one-step spin-coating. First, the PbBr<sub>2</sub> powder was dissolved in a concentrated hydrobromic acid (HBr) to form a pale yellow solution. Then, the CsBr aqueous solution was added dropwise to the as-formed PbBr<sub>2</sub>–HBr solution leading to orange precipitates. After filtering and washing, one can obtain a pure phase CsPbBr<sub>3</sub> powder.<sup>28</sup> As shown in Fig. S1,† the XRD data is well consistent with a standard monoclinic phase of CsPbBr<sub>3</sub> (PDF# 18-0364), and the scanning electron microscopy (SEM) image shows particles of micrometers in size. Additionally, the as-prepared CsPbBr<sub>3</sub> powder can be dissolved in DMSO appearing as a transparent and colorless solution (middle panel of Fig. 1a), making it possible to fabricate the corresponding thin film by a simple one-step method. Interestingly, as shown in the middle images of Fig. 1a, we can observe not only the Tyndall effect but also a green emission when a blue laser (405 nm) is passed through the as-prepared CsPbBr<sub>3</sub> precursor solution, indicating that it is a colloid solution containing some green-emitting particles. Fig. 1b displays the PL spectra of DMSO and DMSO + CsPbBr<sub>3</sub> solution, where we can see that the DMSO solvent exhibits a

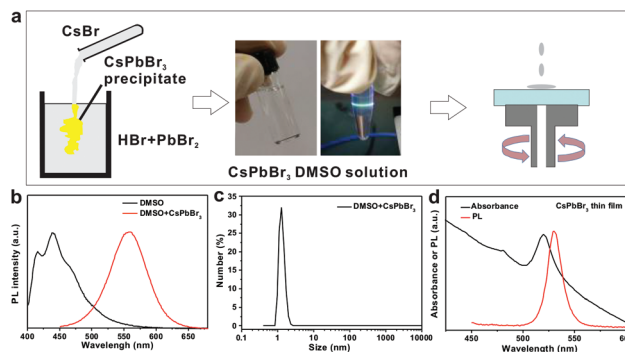


**Fig. 1** One-step solution-processed CsPbBr<sub>3</sub> thin films. (a) Schematic diagrams of preparing CsPbBr<sub>3</sub> powder (left), photographs of the corresponding transparent and colorless CsPbBr<sub>3</sub>–DMSO solution illuminated by normal light and a blue laser of 405 nm (middle) and thin film deposition by spin-coating (right). (b) Photoluminescence (PL) spectra of DMSO and DMSO + CsPbBr<sub>3</sub> solution. (c) Dynamic light scattering spectroscopy of the DMSO + CsPbBr<sub>3</sub> solution. (d) UV-Vis absorption and the PL spectrum of a CsPbBr<sub>3</sub> thin film prepared by one-step spin-coating.

broad emission with two peaks at 416 and 438 nm, showing strong blue luminescence for itself, while the DMSO + CsPbBr<sub>3</sub> solution reveals another broad green emission with a peak at 558 nm, indicating that the green PL observed in Fig. 1a is induced by CsPbBr<sub>3</sub>. As shown in Fig. 1c, dynamic light scattering spectroscopy shows that the DMSO + CsPbBr<sub>3</sub> solution is a colloid solution with a very small average particle size (1.2 nm) and a narrow size distribution. After preparing the DMSO + CsPbBr<sub>3</sub> precursor solution, one can obtain CsPbBr<sub>3</sub> thin films by simply spin-coating this clear solution. Fig. 1d shows typical UV-Vis absorption and PL spectra of the as-deposited CsPbBr<sub>3</sub> thin film; the film exhibits a pronounced exciton absorption peak at 520 nm and a PL peak at 530 nm.

The as-prepared CsPbBr<sub>3</sub> thin films have weak PL emission and we can barely observe the PL when the films were exposed to UV irradiance. We measured the absolute PLQY using an intergraded sphere to quantify the absorbed photons and emission photons. Then, the PLQY was calculated as the ratio of the emission photon number and the absorbed photon number. The PLQY was measured to be ~0.5% for the as-prepared CsPbBr<sub>3</sub> film (Fig. S2†), which is not good enough for LEDs. As it has been proven that the optimized ratio of PbI<sub>2</sub> and MAI in the precursor solution for solar cells is not simply 1 : 1,<sup>1,29</sup> we considered that the PL of the CsPbBr<sub>3</sub> thin film can be possibly tuned by adding PbBr<sub>2</sub> or CsBr into the DMSO + CsPbBr<sub>3</sub> precursor solution. Fig. 2a shows the PL intensity as a function of the CsBr additive amount, in which the positive X axis corresponds to the CsBr additive amount while the negative value corresponds to the PbBr<sub>2</sub> additive amount. Specifically, –0.1 represents a recipe of adding 0.1 mol of PbBr<sub>2</sub> to the as-prepared CsPbBr<sub>3</sub> (1 mol) precursor solution, and 0.2 means adding 0.2 mol of CsBr to the as-prepared CsPbBr<sub>3</sub> (1 mol) precursor solution. It can be seen that adding some amount of PbBr<sub>2</sub> to the pristine CsPbBr<sub>3</sub> pre-

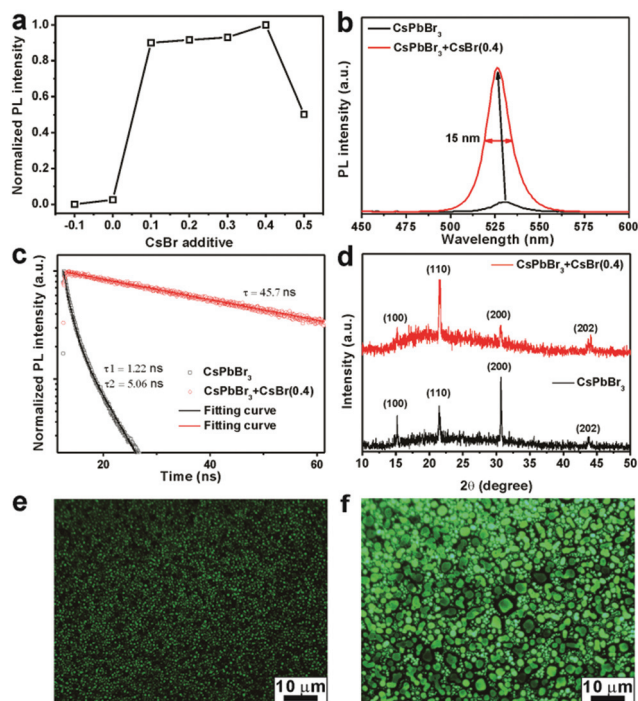


**Fig. 2** Compositional engineering of the CsPbBr<sub>3</sub>-based precursor solution for highly luminous perovskite films. (a) Normalized PL intensity versus the CsBr additive, indicating an optimized PL peak with the 0.4 mol CsBr additive (represented as CsPbBr<sub>3</sub> + CsBr(0.4)). (b) PL spectra, (c) time-resolved PL spectra and (d) XRD patterns of the pristine CsPbBr<sub>3</sub> and the optimized CsPbBr<sub>3</sub> + CsBr(0.4) thin films. (e) and (f) Fluorescence photographs of the pristine CsPbBr<sub>3</sub> and the optimized CsPbBr<sub>3</sub> + CsBr(0.4) thin films.

cursor solution will quench the PL of the corresponding perovskite film. By contrast, after adding some amount of CsBr into the precursor solution, the PL intensity of the corresponding perovskite films is significantly enhanced with an optimized CsBr additive of 0.4 mol, and the corresponding perovskite films are represented as CsPbBr<sub>3</sub> + CsBr(0.4). However, the CsBr additive of more than 0.4 mol will induce PL quenching. The PL spectra of the pristine CsPbBr<sub>3</sub> and CsPbBr<sub>3</sub> + CsBr(0.4) thin films are shown in Fig. 2b, where we observe that the CsBr additive significantly enhances the PL intensity and also induces a slight blue-shift in the emission peak (from 530 to 526 nm). To understand the reasons for PL enhancement induced by adding the CsBr additive, time-resolved PL (TRPL) spectra were recorded and are shown in Fig. 2c. We observe that the TRPL curve of the neat CsPbBr<sub>3</sub> film can be two-exponent fitted and the radiative recombination lifetime ( $\tau_2$ ) is 5.06 ns, similar to previous reports.<sup>19,20</sup> And the TRPL curve of the CsPbBr<sub>3</sub> + CsBr(0.4) film can be one-exponent fitted well and the lifetime is 45.7 ns, which is nearly 4–10 times higher than the pure CsPbBr<sub>3</sub> film and other reports.<sup>19,20</sup> Hence we propose that the Br-rich surface can passivate surface traps, reduce non-radiative recombination and result in PL enhancement, which is also consistent with previous reports.<sup>19</sup> As shown in Fig. S2,† the PLQY of the CsPbBr<sub>3</sub>

+ CsBr(0.4) film is 33.6%, which is 67 times higher than the pristine CsPbBr<sub>3</sub> thin film (0.5%). The XRD data of the above two films are shown in Fig. 2d, and for direct comparison, some other related standard diffraction patterns are shown in Fig. S3 and S4,† from which we can see that both films indicate a monoclinic CsPbBr<sub>3</sub> phase (PDF# 18-0364) and no CsBr residues were observed. By comparing the XRD patterns especially the intensity change of peaks, we conclude that the CsBr additive induces a directional crystal growth along the (110) facet, which may allow for a plate-like morphology.

To probe the surface morphology of the as-prepared perovskite films, fluorescence photographs were recorded and presented in Fig. 2e and f. It is important to note that the images are not taken under the same intensity of UV excitation light. More specifically, the PL of the pristine CsPbBr<sub>3</sub> thin film is too weak to observe and need to be excited with 100% of UV intensity, while the image of the CsPbBr<sub>3</sub> + CsBr(0.4) film is taken with only 5% of excitation UV intensity. Fluorescence microscopy suggests that the neat CsPbBr<sub>3</sub> film consists of polycrystalline islands smaller in size (hundreds of nanometers). By contrast, the CsPbBr<sub>3</sub> + CsBr(0.4) film is made up of larger plate-like particles in the size of several micrometers, which is in agreement with the XRD data (Fig. 2d). Another salient advantage of the as-prepared perovskite thin films is their outstanding ambient stability. As shown in Fig. S5,† the PL spectra of a CsPbBr<sub>3</sub> + CsBr(0.4) film nearly remain the same even after storage in ambient air (~50% humidity) for 3 months. It is believed that the large crystal size (micro-plates) may help to resist moisture penetration and improve stability.<sup>30,31</sup>

After the investigation of CsBr additive's effect on the PL and morphology, the perovskite thin films were employed as emission layers and used to fabricate LEDs. Fig. 3a schematically shows the energy level diagram of the as-fabricated LEDs and the corresponding cross sectional SEM image is shown in Fig. S6,† where an ITO glass serves as the anode, PEDOT:PSS acts as the hole transport layer (HTL) owing to its suitable work function (5.0 eV) and versatile process, B3PYMPM (4,6-bis(3,5-di(pyridin-3-yl)phenyl)-2-methylpyrimidine) is used as the electron transport layer (ETL) as its conduction band matches the perovskite's conduction band well, and CsCO<sub>3</sub> is used as the buffer layer together with Al as the cathode for efficient electron injection. Fig. 3b displays a photograph of the as-fabricated LEDs, revealing three uniform and bright emitting devices, each with an area of 2.0 × 1.5 mm<sup>2</sup>. The top-view SEM images of the CsPbBr<sub>3</sub> and CsPbBr<sub>3</sub> + CsBr(0.4) films deposited on PEDOT:PSS are shown in Fig. S7a and S7b,† respectively. As shown in Fig. S7a,† there are two kinds of polycrystalline domains observed in the as-fabricated CsPbBr<sub>3</sub> thin film, *i.e.*, dot-like small crystalline domains and sparse incomplete cuboid microparticles, and the surface coverage is poor due to the existence of cracks. It is noticeable that the surface morphology shown in Fig. S7a† is not ideal for LED application as the cracks will become the leakage points and reduce performance. By contrast, after adding some CsBr additive, Fig. S7b† shows a higher surface coverage with well-

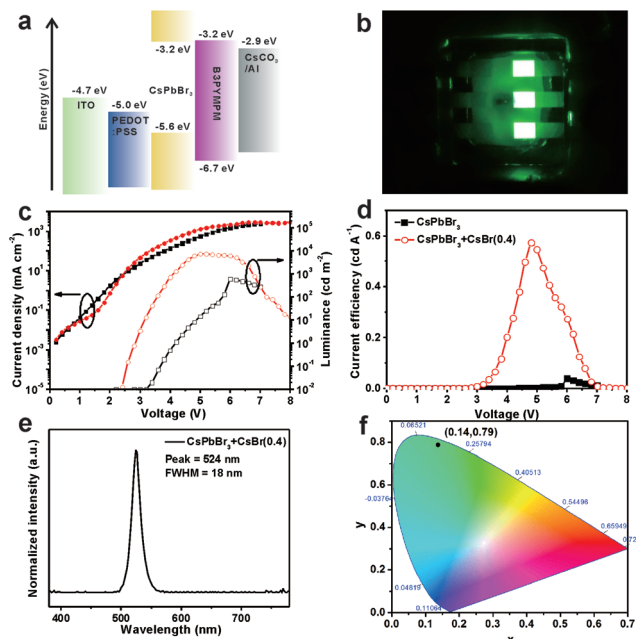


**Fig. 3** Fabrication and characterization of CsPbBr<sub>3</sub>-based LEDs. (a) Energy level diagram and (b) the photograph of the as-fabricated CsPbBr<sub>3</sub>-based devices in operation. (c) Luminance–current density–voltage (*L–J–V*) curves and (d) current efficiency versus applied voltage (*CE–V*) curves of the as-fabricated LEDs. (e) Electroluminescence spectrum of the as-fabricated LED with an emission layer of the CsPbBr<sub>3</sub> + CsBr(0.4) film with an applied voltage of 4 V and (f) the corresponding CIE coordinates.

defined crystalline closely packed micro-cubes, which is good for LED application. To evaluate their LED performance, luminance–current density–voltage (*L–J–V*) curves were recorded and are presented in Fig. 3c. From the *J–V* curves, we notice that the CsPbBr<sub>3</sub> + CsBr(0.4) device shows a better diode characteristics and higher current density (beyond 2.5 V) than the pristine CsPbBr<sub>3</sub> device. We infer from the *L–V* curves that the pure CsPbBr<sub>3</sub> device shows a turn-on voltage (*V*<sub>on</sub>) of 4.2 V and a maximum luminance of 567 cd m<sup>−2</sup> at 6.0 V, which is similar to the previous reports.<sup>4,5,20</sup> The CsPbBr<sub>3</sub> + CsBr(0.4) device reveals a much lower *V*<sub>on</sub> of 2.8 V and a maximum luminance of 7276 cd m<sup>−2</sup> at 5.2 V, which are the lowest *V*<sub>on</sub> and the highest luminance reported in the literature, respectively. The low *V*<sub>on</sub> may be attributed to better electron injection from

the ETL to the perovskite due to the better energy alignment (Fig. 3a). Meanwhile, the performance of some other perovskite LEDs fabricated with different precursor solutions, like CsPbBr<sub>3</sub> + CsBr(0.2), *etc.*, is shown in Fig. S8.† It can be seen that the CsPbBr<sub>3</sub> + CsBr(0.4) out-performs among all the devices, consistent with the previous PL optimization results (Fig. 2a). Fig. 3d shows the current efficiency (*CE*) versus applied voltage, indicating an improved *CE* from 0.04 cd A<sup>−1</sup> without additives to 0.57 cd A<sup>−1</sup> with additives. For direct comparison, some LED characteristics from our work and other related reports are summarized in Table 1, from which we can see that the performance shown here is among the best values reported, especially for the high luminance of 7276 cd m<sup>−2</sup>. Fig. 3e presents the electroluminescence (*EL*) curve of a CsPbBr<sub>3</sub> + CsBr(0.4) device with a driving voltage of 4.0 V, showing a symmetric emission peak at 524 nm with a FWHM of 18 nm, which is one of the narrowest values reported yet.<sup>4</sup> As shown in Fig. 3f, the *EL* corresponds to the Commission Internationale de l'Éclairage (*CIE*) color coordinates of (0.14, 0.79), which is pure green.

Moreover, the external quantum efficiency (*EQE*) can be expressed as the ratio of emitted photons and charge carriers injected:

$$EQE = \frac{P_0/h\nu}{I/e}$$

where *P*<sub>0</sub> is the optical output power (measured by using a calibrated photo-spectrometer), *hν* is the photon energy at the emission frequency *ν*, *I* is the injection current, and *e* is the electron charge. By combining the performance result and *EL* spectra, the maximum *EQE* of the as-fabricated CsPbBr<sub>3</sub> + CsBr(0.4) device is determined to be 0.15%, which is also among the best performances reported.

As mentioned above, the as-fabricated CsPbBr<sub>3</sub> + CsBr(0.4) thin film showed an outstanding *PL* stability in ambient air (Fig. S5†). Hence, we believe that the corresponding LEDs may perform well from a long-term stability point of view. To evaluate the ambient stability of the as-fabricated LEDs, we applied a constant current to the device and recorded the corresponding luminance intensity as a function of time. As well accepted, LED performance stability with an output of 100 cd m<sup>−2</sup> is an important index for practical LEDs.<sup>32</sup> To evaluate our device stability, we applied a constant current

**Table 1** CsPbBr<sub>3</sub>-based LED characteristic comparison of our work and other previous reports

Reports	Emission material	<i>V</i> <sub>on</sub> (V)	<i>L</i> <sub>max</sub> (cd m <sup>−2</sup> )	<i>CE</i> <sub>max</sub> (cd A <sup>−1</sup> )	Stability performance ( <i>T</i> <sub>50</sub> , min)
Yantara <i>et al.</i> <sup>20</sup>	Planar film	3.0	407	0.035	N.A.
Song <i>et al.</i> <sup>5</sup>	NPs	4.2	946	0.43	N.A.
Zhang <i>et al.</i> <sup>4</sup>	NPs	3.5	1377	0.19	10 min in glovebox ( <i>V</i> <sub>app</sub> = 5 V)
Li <i>et al.</i> <sup>7</sup>	NPs	2.8	2335	0.28	N.A.
Our work	Planar film	2.8	7276	0.57	Stable <i>L</i> > 100 cd m <sup>−2</sup> for >15 h in ambient air ( <i>J</i> <sub>app</sub> = 66.67 mA cm <sup>−2</sup> )

NPs (nanoparticles), *V*<sub>on</sub> (turn-on voltage), *L* (luminance), *CE* (current efficiency), N.A. (not applicable), *V*<sub>app</sub> (applied voltage) and *J*<sub>app</sub> (applied current density).

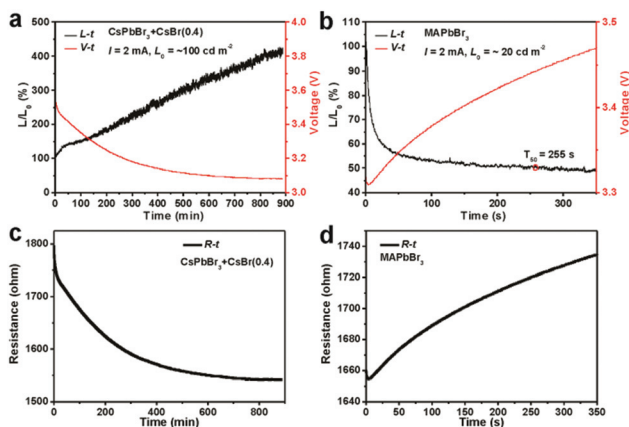


**Fig. 4** Ambient stability investigation of  $\text{CH}_3\text{NH}_3\text{PbBr}_3$  and  $\text{CsPbBr}_3$ -based LEDs. (a) Relative luminance intensity versus time ( $L-t$ ) and voltage versus time ( $V-t$ ) characteristics of  $\text{CsPbBr}_3$ -based LEDs with a constant driving current of 2 mA (corresponding to a current density of  $66.67 \text{ mA cm}^{-2}$ ). (b)  $L-t$  and  $V-t$  characteristics of a  $\text{CH}_3\text{NH}_3\text{PbBr}_3$ -based LED tested under the same testing conditions as  $\text{CsPbBr}_3$ -based LEDs ( $L_0$ : the starting luminance). (c) and (d) Resistance versus time ( $R-t$ ) characteristics of the  $\text{CsPbBr}_3$  and  $\text{MAPbBr}_3$ -based LEDs.

to the device, ensured the starting luminance is around  $100 \text{ cd m}^{-2}$  and recorded the luminance output and applied voltage evolution as a function of time. As shown in the relative luminance intensity versus the time ( $L-t$ ) curve of Fig. 4a, the  $\text{CsPbBr}_3 + \text{CsBr}(0.4)$  device shows stable performance over more than 15 h under a constant driving current of 2 mA ( $J = 66.67 \text{ mA cm}^{-2}$ ) without any degradation but instead exhibits a steadily increasing luminance trend from around  $100$  to  $400 \text{ cd m}^{-2}$ . For direct comparison, a  $\text{MAPbBr}_3$ -based LED device was fabricated and tested under the same conditions, and the corresponding  $L-J-V$  curve is shown in Fig. S9.† The as-fabricated  $\text{MAPbBr}_3$ -based LED shows a maximum luminance of  $330 \text{ cd m}^{-2}$  at 5 V, similar to the previous reports.<sup>8,9</sup> However, when the device is driven with a constant current of 2 mA, as shown in Fig. 4b, the luminance intensity decreases rapidly. We define the half-lifetime ( $T_{50}$ ) as the time for the luminance decreasing to 50% of the starting luminance ( $L_0$ ). Accordingly, the  $T_{50}$  of the as-fabricated  $\text{MAPbBr}_3$  device is only 255 s, which is still far from practical LED applications. As the applied current is fixed at 2 mA, the voltage versus time ( $V-t$ ) curves in Fig. 4a and b can be easily converted into  $R-t$  curves (resistance versus time) by the equation  $R = V/I$ . From the  $R-t$  curve shown in Fig. 4c, we can see that the overall resistance of the  $\text{CsPbBr}_3 + \text{CsBr}(0.4)$  device drops slightly with time. As there is no chemical reaction or phase transfer in the device, we propose that the decreasing of device resistance is due to the interface contact improvement (ETL/perovskite/HTL) or perovskite crystalline film annealing caused by joule heating. And the decrease of device resistance (joule heating induced annealing effect) should be also the reason for the luminance increasing as shown in Fig. 4a. The joule heat ( $Q$ ) can be calculated with the equation  $Q = I^2Rt$ , and the  $R-t$  curve of the  $\text{MAPbBr}_3$  device (Fig. 4d) shows that the resistance is growing,

meaning that the device may be overheated by the joule heat. As a result, we believe that the  $\text{MAPbBr}_3$  perovskite will decompose due to the increasing joule heat. In other words, the instability of the  $\text{MAPbBr}_3$  device may be attributed to the decomposition of  $\text{MAPbBr}_3$  perovskites caused by joule heat under high current flowing.<sup>33</sup> By contrast, the  $\text{CsPbBr}_3$  perovskites have been proved to be more thermally-stable compared to the common  $\text{MAPbBr}_3$  perovskites,<sup>16–18</sup> which may contribute to the superior device performance stability.

Besides evaluating LED stability at  $L_0$  of  $100 \text{ cd m}^{-2}$ , we further investigated the device stability when it was operated at a higher luminance. As shown in Fig. S10,† when the applied current was increased to 10 mA,  $L_0$  jumped to  $\sim 700 \text{ cd m}^{-2}$ . However, the corresponding performance is not stable, as the initial luminance decrease to 60% of  $L_0$  in 100 min. Nonetheless, all our results unambiguously showed that the  $\text{CsPbBr}_3$  LEDs can perform stably at least with  $L > 100 \text{ cd m}^{-2}$ , which is definitely an important milestone in this field.

## Conclusions

To conclude, we have successfully fabricated highly bright and durable  $\text{CsPbBr}_3$ -based LEDs, where the perovskite film is prepared by a simple one-step solution method under the ambient conditions. It is believed that the superior performance is attributed to the non-stoichiometric  $\text{CsPbBr}_3$  precursor solution with the CsBr additive, where the CsBr additive not only passivates the particle surface trap to enhance PLQY but also induces directional crystal growth into micro-plates. The as-fabricated highly luminous perovskite films, when applied as emitting layers in LEDs, show a record high brightness of  $7276 \text{ cd m}^{-2}$  and excellent color purity (FWHM = 18 nm). According to the efficiency gaining process for inorganic/organic perovskite solar cells,<sup>1,2,16</sup> our developed one-step solution method is expected to continually improve LED performance by modifying the precursor solution. More importantly, the as-fabricated perovskite LEDs show incredible ambient stability with a luminance output of  $>100 \text{ cd m}^{-2}$  (steady increase without any degradation trend) for at least 15 h, suggesting considerable potential promise towards developing practical LEDs for lighting and displays.

## Acknowledgements

Q. H. Xiong gratefully acknowledges the strong support for this work from the Singapore National Research Foundation through an Investigatorship Award (NRF-NRFI2015-03), Ministry of Education via two AcRF Tier 2 grants (MOE2013-T2-1-049 and MOE2015-T2-1-047) and Tier 1 grant (2013-T1-002-232). H. V. D. is pleased to acknowledge the Singapore National Research Foundation through an Investigatorship Award (NRF-NRFI2016-08) and Competitive Research Programme (CRP Award No. NRF-CRP14-2014-03).

## Notes and references

- 1 D. Bi, W. Tress, M. I. Dar, P. Gao, J. Luo, C. Renevier, K. Schenk, A. Abate, F. Giordano, J. P. Correa Baena, J. D. Decoppet, S. M. Zakeeruddin, M. K. Nazeeruddin, M. Gratzel and A. Hagfeldt, *Sci. Adv.*, 2016, **2**, e1501170.
- 2 N. J. Jeon, J. H. Noh, W. S. Yang, Y. C. Kim, S. Ryu, J. Seo and S. I. Seok, *Nature*, 2015, **517**, 476–480.
- 3 W. Chen, Y. Wu, Y. Yue, J. Liu, W. Zhang, X. Yang, H. Chen, E. Bi, I. Ashraful, M. Gratzel and L. Han, *Science*, 2015, **350**, 944–948.
- 4 X. Zhang, H. Lin, H. Huang, C. Reckmeier, Y. Zhang, W. C. Choy and A. L. Rogach, *Nano Lett.*, 2016, **16**, 1415–1420.
- 5 J. Song, J. Li, X. Li, L. Xu, Y. Dong and H. Zeng, *Adv. Mater.*, 2015, **27**, 7162–7167.
- 6 J. Wang, N. Wang, Y. Jin, J. Si, Z. K. Tan, H. Du, L. Cheng, X. Dai, S. Bai, H. He, Z. Ye, M. L. Lai, R. H. Friend and W. Huang, *Adv. Mater.*, 2015, **27**, 2311–2316.
- 7 G. Li, F. W. Rivarola, N. J. Davis, S. Bai, T. C. Jellicoe, F. de la Pena, S. Hou, C. Ducati, F. Gao, R. H. Friend, N. C. Greenham and Z. K. Tan, *Adv. Mater.*, 2016, **28**, 3528–3534.
- 8 G. Li, Z. K. Tan, D. Di, M. L. Lai, L. Jiang, J. H. Lim, R. H. Friend and N. C. Greenham, *Nano Lett.*, 2015, **15**, 2640–2644.
- 9 Z. K. Tan, R. S. Moghaddam, M. L. Lai, P. Docampo, R. Higler, F. Deschler, M. Price, A. Sadhanala, L. M. Pazos, D. Credgington, F. Hanusch, T. Bein, H. J. Snaith and R. H. Friend, *Nat. Nanotechnol.*, 2014, **9**, 687–692.
- 10 H. Cho, S.-H. Jeong, M.-H. Park, Y.-H. Kim, C. Wolf, C.-L. Lee, J. H. Heo, A. Sadhanala, N. Myoung, S. Yoo, S. H. Im, R. H. Friend and T.-W. Lee, *Science*, 2015, **350**, 1222–1225.
- 11 Y. H. Kim, H. Cho, J. H. Heo, T. S. Kim, N. Myoung, C. L. Lee, S. H. Im and T. W. Lee, *Adv. Mater.*, 2015, **27**, 1248–1254.
- 12 H. Chen, Z. Wei, H. He, X. Zheng, K. S. Wong and S. Yang, *Adv. Energy Mater.*, 2016, **6**, 1502087.
- 13 Z. Wei, X. Zheng, H. Chen, X. Long, Z. Wang and S. Yang, *J. Mater. Chem. A*, 2015, **3**, 16430–16434.
- 14 Z. Wei, H. Chen, K. Yan and S. Yang, *Angew. Chem., Int. Ed.*, 2014, **53**, 13239–13243.
- 15 Z. Wei, K. Yan, H. Chen, Y. Yi, T. Zhang, X. Long, J. Li, L. Zhang, J. Wang and S. Yang, *Energy Environ. Sci.*, 2014, **7**, 3326–3333.
- 16 M. Saliba, T. Matsui, J.-Y. Seo, K. Domanski, J.-P. Correa-Baena, M. K. Nazeeruddin, S. M. Zakeeruddin, W. Tress, A. Abate, A. Hagfeldt and M. Grätzel, *Energy Environ. Sci.*, 2016, **9**, 1989–1997.
- 17 R. J. Sutton, G. E. Eperon, L. Miranda, E. S. Parrott, B. A. Kamino, J. B. Patel, M. T. Hörantner, M. B. Johnston, A. A. Haghighirad, D. T. Moore and H. J. Snaith, *Adv. Energy Mater.*, 2016, **6**, 1502458.
- 18 D. P. McMeekin, G. Sadoughi, W. Rehman, G. E. Eperon, M. Saliba, M. T. Hörantner, A. Haghighirad, N. Sakai, L. Korte, B. Rech, M. B. Johnston, L. M. Herz and H. J. Snaith, *Science*, 2016, **351**, 151–155.
- 19 X. Li, Y. Wu, S. Zhang, B. Cai, Y. Gu, J. Song and H. Zeng, *Adv. Funct. Mater.*, 2016, **26**, 2435–2445.
- 20 N. Yantara, S. Bhaumik, F. Yan, D. Sabba, H. A. Dewi, N. Mathews, P. P. Boix, H. V. Demir and S. Mhaisalkar, *J. Phys. Chem. Lett.*, 2015, **6**, 4360–4364.
- 21 Y. Deng, E. Peng, Y. Shao, Z. Xiao, Q. Dong and J. Huang, *Energy Environ. Sci.*, 2015, **8**, 1544–1550.
- 22 N. J. Jeon, J. H. Noh, Y. C. Kim, W. S. Yang, S. Ryu and S. I. Seok, *Nat. Mater.*, 2014, **13**, 897–903.
- 23 M. Kulbak, D. Cahen and G. Hodes, *J. Phys. Chem. Lett.*, 2015, 2452–2456, DOI: 10.1021/acs.jpcclett.5b00968.
- 24 L. Protesescu, S. Yakunin, M. I. Bodnarchuk, F. Krieg, R. Caputo, C. H. Hendon, R. X. Yang, A. Walsh and M. V. Kovalenko, *Nano Lett.*, 2015, **15**, 3692–3696.
- 25 G. Nedelcu, L. Protesescu, S. Yakunin, M. I. Bodnarchuk, M. J. Grotevent and M. V. Kovalenko, *Nano Lett.*, 2015, **15**, 5635–5640.
- 26 Q. A. Akkerman, V. D’Innocenzo, S. Accornero, A. Scarpellini, A. Petrozza, M. Prato and L. Manna, *J. Am. Chem. Soc.*, 2015, **137**, 10276–10281.
- 27 J. Burschka, N. Pellet, S. J. Moon, R. Humphry-Baker, P. Gao, M. K. Nazeeruddin and M. Gratzel, *Nature*, 2013, **499**, 316–318.
- 28 C. C. Stoumpos, C. D. Malliakas, J. A. Peters, Z. Liu, M. Sebastian, J. Im, T. C. Chasapis, A. C. Wibowo, D. Y. Chung, A. J. Freeman, B. W. Wessels and M. G. Kanatzidis, *Cryst. Growth Des.*, 2013, **13**, 2722–2727.
- 29 Y. C. Kim, N. J. Jeon, J. H. Noh, W. S. Yang, J. Seo, J. S. Yun, A. Ho-Baillie, S. Huang, M. A. Green, J. Seidel, T. K. Ahn and S. I. Seok, *Adv. Energy Mater.*, 2016, **6**, 1502104.
- 30 J. H. Kim, S. T. Williams, N. Cho, C.-C. Chueh and A. K. Y. Jen, *Adv. Energy Mater.*, 2015, **5**, 1401229.
- 31 Z. Yang, C.-C. Chueh, F. Zuo, J. H. Kim, P.-W. Liang and A. K. Y. Jen, *Adv. Energy Mater.*, 2015, **5**, 1500328.
- 32 X. Dai, Z. Zhang, Y. Jin, Y. Niu, H. Cao, X. Liang, L. Chen, J. Wang and X. Peng, *Nature*, 2014, **515**, 96–99.
- 33 J. C. Yu, D. W. Kim, B. Kim da, E. D. Jung, J. H. Park, A. Y. Lee, B. R. Lee, D. Di Nuzzo, R. H. Friend and M. H. Song, *Adv. Mater.*, 2016, **28**, 6906–6913.